NASA-CR-200890

# *CONTROL OF UNSTABLE WAVES IN THREE DIMENSIONAL BOUNDARY LAYERS*

Final Technical Report
Full Award Period 2/23/90 - 5/15/95

*SPONSOR AWARD # NAG-1-1111*

NASA-Langley Research Center
Chief Scientist
Mail Stop 110
Hampton, VA. 23665-5225

Attention:
Mr. Dennis M. Bushnell

APRIL 1996

Submitted by

WILLIAM S. SARIC

Mechanical and Aerospace Engineering
College of Engineering and Applied Science
Arizona State University
Tempe, AZ 85287-6106

---

Janice D. Bennett, Director
Office of Research Creative Activity
(602) 965-8239

Mark S. Reibert† and William S. Saric†

# Control of unstable waves in three-dimensional boundary layers

## Abstract

Stability experiments are conducted in the Arizona State University Unsteady Wind Tunnel on a 45° swept airfoil. The pressure gradient is designed to provide purely crossflow-dominated transition; that is, the boundary layer is subcritical to Tollmien-Schlichting (T-S) disturbances. The airfoil surface is hand polished to a 0.25 $\mu$m rms finish. Under these conditions, stationary crossflow disturbances grow to nonuniform amplitude due to submicron surface irregularities near the leading edge. Spectral decompositions isolate single-mode growth rates for the fundamental and harmonic disturbances. The measurements show early nonlinear growth causing amplitude saturation well before transition. Comparisons with nonlinear PSE calculations show excellent agreement in both the amplitude saturation and the disturbance mode shape.

## Background and motivation

The present swept-wing research program experimentally investigates the fundamental nature of the crossflow instability which leads to transition in three-dimensional boundary layers. Gregory et al. (1955) provide the theoretical basis for the instability. It results in an Orr-Sommerfeld type solution that can be implemented in a variety of ways. See Mack (1984) for the development of the details of the instability. Reed and Saric (1989), Saric (1992b) and Arnal (1992) review the literature.

### *Fundamentals*

In contrast to Tollmien-Schlichting (T-S) instabilities, the crossflow problem exhibits stationary ($f = 0$) as well as traveling disturbances. The traveling waves are more amplified according to linear theory, however many experiments are dominated by stationary waves. Müller and Bippes (1989), Bippes (1990, 1991), Bippes et al. (1991), and Deyhle and Bippes (1996) have shown that traveling waves are observed in tunnels rich in unsteady freestream disturbances, whereas stationary waves dominate in a low-turbulence environment. Since the flight environment is more benign than the wind tunnel, one expects the low-turbulence results to be more important.

Mark S. Reibert† and William S. Saric†

# Control of unstable waves in three-dimensional boundary layers

## Abstract

Stability experiments are conducted in the Arizona State University Unsteady Wind Tunnel on a 45° swept airfoil. The pressure gradient is designed to provide purely crossflow-dominated transition; that is, the boundary layer is subcritical to Tollmien-Schlichting (T-S) disturbances. The airfoil surface is hand polished to a 0.25 $\mu$m rms finish. Under these conditions, stationary crossflow disturbances grow to nonuniform amplitude due to submicron surface irregularities near the leading edge. Spectral decompositions isolate single-mode growth rates for the fundamental and harmonic disturbances. The measurements show early nonlinear growth causing amplitude saturation well before transition. Comparisons with nonlinear PSE calculations show excellent agreement in both the amplitude saturation and the disturbance mode shape.

## Background and motivation

The present swept-wing research program experimentally investigates the fundamental nature of the crossflow instability which leads to transition in three-dimensional boundary layers. Gregory et al. (1955) provide the theoretical basis for the instability. It results in an Orr-Sommerfeld type solution that can be implemented in a variety of ways. See Mack (1984) for the development of the details of the instability. Reed and Saric (1989), Saric (1992b) and Arnal (1992) review the literature.

### *Fundamentals*

In contrast to Tollmien-Schlichting (T-S) instabilities, the crossflow problem exhibits stationary ($f = 0$) as well as traveling disturbances. The traveling waves are more amplified according to linear theory, however many experiments are dominated by stationary waves. Müller and Bippes (1989), Bippes (1990, 1991), Bippes et al. (1991), and Deyhle and Bippes (1996) have shown that traveling waves are observed in tunnels rich in unsteady freestream disturbances, whereas stationary waves dominate in a low-turbulence environment. Since the flight environment is more benign than the wind tunnel, one expects the low-turbulence results to be more important.

One of the important results to come out of the DLR experiments is the set of data that show early saturation of the stationary disturbance amplitude and the failure of linear theory to predict the growth of the instability (Bippes and Nitschke-Kowsky 1990; Bippes et al. 1991; Deyhle et al. 1993). Dagenhart et al. (1989, 1990) and Radeztsky et al. (1994) observed similar behavior. Kohama et al. (1991) showed that the *stationary* crossflow vortex controls transition by causing a high-frequency secondary instability resulting from the nonlinear mean-flow distortion. More recently, Deyhle and Bippes (1996) document the role of freestream disturbances with regard to traveling crossflow waves. Radeztsky et al. (1993) show that the receptivity process for stationary waves is strongly influenced by surface roughness, i.e., initial amplitudes. Insofar as stationary crossflow waves are concerned, it is clear that a successful transition prediction scheme must account for the initial conditions and the nonlinear growth of the disturbance. It is this aspect of the problem which we address in this paper.

### *Objectives*

In earlier ASU experiments, Dagenhart et al. (1989, 1990) found that naturally occurring stationary crossflow waves of moderate amplitude have lower growth rates than predicted by linear theory. Under the same conditions, Radeztsky et al. (1993) investigated the sensitivity to surface roughness and showed early saturation of the natural stationary disturbance amplitude. Later experiments by Radeztsky et al. (1994) examined the growth of very weak crossflow waves in an attempt to close the gap between previous experimental results and linear theory. Even for these weak waves, linear theory completely failed to predict the disturbance growth.

In all of the early experiments measuring the growth of the stationary crossflow wave (Dagenhart et al. 1989, 1990; Bippes et al. 1991), the initial conditions for the disturbance amplitude came from the unknown natural roughness of the surface. Although a dominant wavelength appears, the resulting stationary structure is nonuniform in span and contains many fundamental disturbance modes of unknown amplitude. Consequently, comparisons with single-mode numerical predictions are not possible.

The same NLF(2)-0415 airfoil (Somers and Horstmann 1985) is used as in the previous experiments. With a 45° sweep and a $-4°$ angle of attack, the favorable pressure gradient produces considerable crossflow while suppressing T-S modes. Arrays of 6 $\mu$m roughness elements near the leading edge produce *uniform* stationary disturbances without excessive initial amplitudes. Spectral techniques are used to identify and follow specific stationary modes, thus providing single-wavelength growth rates for comparison with theoretical calculations.

## The experiment

### *Facility and model*

The Unsteady Wind Tunnel at Arizona State University is a low-speed, low-turbulence, closed-circuit facility used to study the stability and transition of laminar boundary

layers (Saric 1992a). The airfoil model is mounted vertically in the 1.4 m × 1.4 m × 5 m test section. The aluminum surface is hand polished to a 0.25 $\mu$m rms finish so that even micron-sized roughness elements are well above the background roughness level.

*Measurement techniques*

Two standard hot-wire scanning methods are used to investigate the stationary crossflow waves. These are described below.

Wall-normal scans

Wall-normal boundary-layer scans provide a detailed map of the stationary structure. These maps are constructed by taking a spanwise series of mean-flow boundary-layer profiles at constant $x/c$. Once the scans are aligned with the airfoil surface, disturbance profiles are generated from which a stationary crossflow mode shape is computed. The disturbance growth is calculated by tracking the size of the mode shape at various chord positions. Three different measures of the mode shape size are used to characterize the disturbance amplitude: the maximum of the mode, the integral of $|u'|$ with respect to $y$, and the integral of $|u'|^2$ with respect to $y$. When the disturbance growth is cast in terms of the amplification factor $N$, all three measures collapse onto a single $N$-factor curve. These results, however, cannot (in general) be quantitatively compared with single-wavelength linear predictions since all amplified stationary modes are lumped into a single mode shape.

Single-wavelength information can be extracted from a boundary-layer map by taking a spanwise slice across the profiles at a constant height above the airfoil surface. The resulting velocity vs. span trace can be decomposed using spectral techniques to resolve the wavenumber content. Reasonable resolution in the wavenumber domain, however, requires a large spanwise extent of the measurement region. Consequently, this technique can quickly become prohibitively time consuming.

Spanwise scans

Individual-wavelength growth rates are obtained by restricting hot-wire measurements to a single spanwise scan at a constant height above the airfoil surface. With this technique, data are acquired along the entire span of the measurement region (240 mm) at much higher (spanwise) resolution than the wall-normal scans. Since data are collected at only one height in the boundary layer, these scans progress very quickly (typically 75 minutes per scan compared to nearly 45 hours for a full set of wall-normal scans with the same spanwise extent and resolution). The disadvantage of this technique is that the details of the stationary structure are not captured. For this reason, a disturbance mode shape (produced with a small set of wall-normal scans) is used to guide the spanwise scans.

## Results

*Basic state*

The basic state is documented with pressure measurements and mean-flow boundary-layer profiles. Figure 1 shows the measured and theoretical $C_p$ distribution over the airfoil upper surface. The experimental data are the average readings from two sets of pressure ports in the airfoil surface. The theoretical curve is the inviscid solution from the NASA Langley code MCARF. The agreement, especially in terms of the pressure gradient, is good over the entire measurement region.

*Boundary-layer maps*

Figure 2 is a contour plot of the streamwise velocity $u/U_e$ in the $(y, z)$ plane. The flow is toward the reader, and the stationary vortices are turning in the right-handed sense. These data are acquired at $x/c = 0.45$, $Re_c = 3.0 \times 10^6$, with no artificial roughness on the airfoil. The nonuniformity of the naturally occurring stationary waves is caused by submicron surface irregularities near the leading edge. Figure 2 displays a strong feature at a 12 mm spacing, which is approximately the most amplified stationary wavelength. At the same time, the richness in the spectral content is evident. This is typical of all of the earlier data (Bippes and Nitschke-Kowsky 1990; Bippes et al. 1991; Deyhle et al. 1993; Dagenhart et al. 1989, 1990), and indicates both nonlinear behavior and multiple modes. Thus, even a nonlinear calculation that included only a single spanwise mode would be inappropriate to characterize the disturbance motion.

In order to generate spanwise-uniform stationary crossflow waves, initial conditions are controlled by applying a full-span array of roughness elements at $x/c = 0.023$ (near the neutral point of the instability) following Radeztsky et al. (1993). The roughness height is $k = 6$ $\mu$m, and the 3.7 mm diameter elements are spaced 12 mm apart in span, corresponding to the most amplified wavelength according to linear theory. Figure 3 shows the streamwise velocity contours at $x/c = 0.45$ and $Re_c = 2.4 \times 10^6$ with this roughness distribution. Under these conditions, the roughness Reynolds number, $Re_k$, is 0.1. The uniformity of the fundamental 12 mm mode is striking, and allows for meaningful comparisons with single-mode theoretical predictions. A single vortex is isolated in Figure 4 and plotted on a 1:1 scale. The crossflow vortex produces regions of upwelling and downwelling which transport low- and high-momentum fluid, respectively. The symmetry of the co-rotating vortex distorts this momentum transfer giving an apparent rollover of low-momentum fluid that appears above high-momentum fluid.

Figure 5 shows the 100 boundary-layer profiles from which Figure 3 is generated. The profiles are obtained at 1 mm intervals in the swept span direction. The dots indicate the spanwise average of the profiles, which accounts for basic state plus the mean-flow distortion [(0, 0) mode]. It should be emphasized that these are mean profiles and not an unsteady oscillation in the boundary layer. One can clearly see how the stationary vortex structure has distorted the mean flow, resulting in accelerated, decelerated, and doubly inflected profiles existing millimeters apart. The nonlinearities are indicated by

the distortion of the averaged profile in the vicinity of $y \approx 2.8$ mm. This distortion of the basic state leads to the secondary instability which controls the transition to turbulence (Kohama et al. 1991).

Disturbance profiles are generated by subtracting the basic state plus mean-flow distortion (i.e., the spanwise average profile) from the individual boundary-layer profiles (Figure 6). From these data, the crossflow mode shape is generated by computing the spanwise rms of the disturbance profiles (Figure 7). This mode shape contains the fundamental disturbance and all amplified harmonics.

The total disturbance amplitude is computed using three measures of the mode shape size as outlined above. Growth rates are obtained by repeating this procedure at several chord positions. Figure 8 shows the disturbance amplitude distribution for 6 $\mu$m roughness with 12 mm spacing at $Re_c = 2.4 \times 10^6$. The dashed lines represent the absolute size of the mode shape as computed by each of the three measures. The solid lines show the corresponding amplification factor $N$. The ability of the $N$-factor to collapse the data onto a single curve is typical. The nonlinear saturation is clearly evident, and occurs well before the transition location of $(x/c)_{\rm tr} = 0.52$. It is worth emphasizing that these measures record the *total* disturbance amplitude since all amplified wavelengths are present in the mode shape.

Figure 9 compares the experimental $N$-factor (as computed from the maximum of the mode shape profiles) with various theoretical predictions of Haynes and Reed (1996). The nonlinear parabolized stability equations (NPSE) results are computed using initial amplitudes provided by the experiment. The agreement is excellent, especially in predicting the amplitude saturation. (At this time, the Haynes and Reed formulation does not contain curvature, which is known to be stabilizing and may account for the small differences in the disturbance growth.) In contrast, the Orr-Sommerfeld and linear PSE results fail to predict the details of the disturbance growth. The early qualitative agreement with the linear PSE results indicates that the nonlinear effects are initially weak up to $x/c = 0.20$, at which time the growth rates depart from linear behavior. It is at this location that the spanwise average of the boundary-layer profiles first begins to exhibit the distortion shown in Figure 5.

*Wavelength separation*

As pointed out previously, crossflow amplitudes computed from mode-shape profiles contain all amplified stationary modes. To decompose the wavenumber content of the disturbance, the spanwise scan technique discussed above is used. Figure 10 shows the spanwise velocity profile at $x/c = 0.45$ for $Re_c = 2.4 \times 10^6$. The roughness configuration is $k = 6$ $\mu$m with 12 mm spanwise spacing. The data are acquired at $y = 0.9$ mm above the airfoil surface, corresponding to the maximum of the mode-shape profile. The strong distortion of the boundary-layer is evident, as is the spanwise uniformity of the stationary structure.

The FFT-based power spectral density (PSD) is shown in Figure 11. The dominance of the fundamental 12 mm mode is clear. However, the superharmonics at $\lambda_s = 6$ mm and 4 mm are also amplified. (The amplitude of the 4 mm mode is too small to appear

on the scale of Figure 11.) This wave doubling was observed by Saric and Yeates (1985) and predicted by Reed (1988). Disturbance amplitudes are computed by integrating the peaks of the PSD. When repeated at several chord positions, the growth rates of Figure 12 are obtained. The dashed lines represent the rms amplitude of the individual modes, while the amplification factor $N$ is plotted with solid lines. At each chord location, the spanwise scan is taken at the boundary-layer height corresponding to the maximum of the mode-shape profile. This permits us to compare the amplitude of the individual modes with that of the total disturbance as computed from the maximum of the mode shape (indicated on Figure 12 by the lines marked "Total"). It is a remarkable verification of the two different measurement techniques that the amplitudes of the total and fundamental ($\lambda_s = 12$ mm) disturbances agree for $x/c < 0.30$. For $x/c > 0.30$, the amplitude of the fundamental diverges from the total disturbance, and the harmonic at $\lambda_s = 6$ mm becomes measurable. In the region of strong nonlinear interaction and amplitude saturation ($x/c \geq 0.35$), the 6 mm component shows significant energy and the 4 mm mode becomes unstable.

## Conclusions

Stationary crossflow waves are investigated on a swept airfoil within a low-disturbance environment. It is shown that even though the surface is polished to 0.25 $\mu$m rms roughness, stationary crossflow waves still dominate the transition process. Because the initial roughness is nonuniform, the resulting disturbance motion is nonuniform and is complicated by the presence of many different modes. Because of this, comparisons with different theoretical and computational schemes are unnecessarily rendered much more difficult.

Systematic introduction of equally spaced 6 $\mu$m roughness elements ($Re_k = 0.1$) is shown to produce an ideal fundamental mode at that spacing. When the roughness elements are placed at the most amplified linear-mode wavelength of $\lambda_s = 12$ mm, disturbance growth, departure from linearity, and saturation amplitude are documented. Evidence of growth at the 6 mm and 4 mm harmonics is shown. There is no evidence of wavelength doubling (i.e., components at 24 mm or 36 mm). Comparisons with computations using nonlinear parabolized stability equations are very good. It is possible to conclude that the introduction of systematic weak roughness provides the necessary data base for comparisons with theory and computations.

These data continue to illustrate the extreme sensitivity to leading-edge roughness. Strong nonlinear distortion of the mean flow is observed, as is the nonlinear saturation of the disturbance amplitude. This saturation occurs well before the transition to turbulence. Linear theory fails to capture these details of the disturbance growth. On the other hand, NPSE calculations agree remarkably well with the experimental data.

## Acknowledgments

This work was supported by NASA Langley Research Center Grant NCC-1-94. Mr. Reibert was supported by NASA Langley Research Center Fellowship NAG-1-1111. Mr. Carrillo was supported by the National Science Foundation Fellowship Program. Mr. Tim Haynes' numerical calculations and technical discussions are gratefully acknowledged. The technical support of Mr. Dan Clevenger is greatly appreciated.

## References

Arnal, D. 1992 — Boundary-layer transition: Prediction, application to drag reduction. In *Special Course on Skin Friction Drag Reduction*, AGARD R-786.

Bippes, H. 1990 — Instability feature appearing on swept wing configurations. In *Laminar-Turbulent Transition* (eds. Arnal, D. and Michel, R.), vol. 3, pp. 419–430. Springer-Verlag, New York.

Bippes, H. 1991 — Experiments on transition in three-dimensional accelerated boundary-layer flows. In *Proc. R.A.S. Boundary Layer Transition and Control*, Cambridge, U.K.

Bippes, H. and Nitschke-Kowsky, P. 1990 — Experimental study of instability modes in a three-dimensional boundary layer. *AIAA J.* **28**(10), 1758–1763.

Bippes, H., Müller, B., and Wagner, M. 1991 — Measurements and stability calculations of the disturbance growth in an unstable three-dimensional boundary layer. *Phys. Fluids* **3**(10), 2371–2377.

Dagenhart, J.R., Saric, W.S., Mousseux, M.C., and Stack, J.P. 1989 — Crossflow vortex instability and transition on a 45-degree swept wing. AIAA Paper 89-1892.

Dagenhart, J.R., Saric, W.S., Hoos, J.A., and Mousseux, M.C. 1990 — Experiments on swept-wing boundary layers. In *Laminar-Turbulent Transition* (eds. Arnal, D. and Michel, R.), vol. 3, pp. 369–380. Springer-Verlag, New York.

Deyhle, H. and Bippes, H. 1996 — Disturbance growth in an unstable three-dimensional boundary layer and its dependence on environmental conditions. To appear in *J. Fluid Mech.*

Deyhle, H., Höhler, G., and Bippes, H. 1993 — Experimental investigation of instability wave propagation in a 3-D boundary-layer flow. *AIAA J.* **31**(4), 637–645.

Gregory, N., Stuart, J.T., and Walker, W.S. 1955 — On the stability of three-dimensional boundary layers with applications to the flow due to a rotating disk. *Phil. Trans. Roy. Soc. Lon. A* **248**(943), 155–199.

Haynes, T.S. and Reed, H.L. 1996 — Computations in nonlinear saturation of stationary crossflow vortices in a swept-wing boundary layer. AIAA Paper 96-0182.

Kohama, Y., Saric, W.S., and Hoos, J.A. 1991 — A high-frequency secondary instability of crossflow vortices that leads to transition. In *Proc. R.A.S. Boundary Layer Transition and Control*, Cambridge, U.K.

Mack, L.M. 1984 — Boundary-layer linear stability theory. In *Special Course on Stability and Transition of Laminar Flows*, AGARD R-709.

Müller, B. and Bippes, H. 1988 — Experimental study of instability modes in a three-dimensional boundary layer. In *Fluid Dynamics of Three-Dimensional Turbulent Shear Flows and Transition*, AGARD CP-438.

Radeztsky, R.H. Jr., Reibert, M.S., Saric, W.S., and Takagi, S. 1993 — Effect of micron-sized roughness on transition in swept-wing flows. AIAA Paper 93-0076.

Radeztsky, R.H. Jr., Reibert, M.S., and Saric, W.S. 1994 — Development of stationary crossflow vortices on a swept wing. AIAA Paper 94-2373.

Reed, H.L. 1988 — Wave interactions in swept-wing flows. *Phys. Fluids* **30**(11), 3419–3426.

Reed, H.L. and Saric, W.S. 1989 — Stability of three-dimensional boundary layers. In *Annual Review of Fluid Mechanics* (eds. Lumley, J.L., Van Dyke, M., and Reed, H.L.), vol. 21, pp. 235–284. Annual Reviews Inc., Palo Alto, California.

Saric, W.S. 1992a — The ASU transition research facility. AIAA Paper 92-3910.

Saric, W.S. 1992b — Laminar-turbulent transition: Fundamentals. In *Special Course on Skin Friction Drag Reduction*, AGARD R-786.

Saric, W.S. and Yeates, L.G. 1985 — Experiments on the stability of crossflow vortices in swept-wing flows. AIAA Paper 85-0493.

Somers, D.M. and Horstmann, K.H. 1985 — Design of a medium-speed natural-laminar-flow airfoil for commuter aircraft applications. *DFVLR-IB/29-85/26.*

†Arizona State University
Mechanical and Aerospace Engineering
Box 87-6106
Tempe, AZ 85287-6106, USA

‡Clarkson University
Mechanical and Aeronautical Engineering
Box 5725
Potsdam, NY 13699-5725, USA

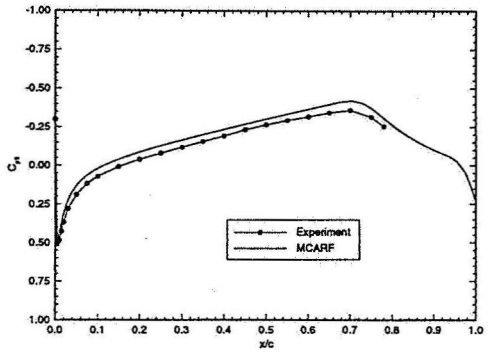


Figure 1: Experimental and theoretical swept $C_p$ distribution at $Re_c = 2.4 \times 10^6$. The theory is computed with the NASA Langley code MCARF.

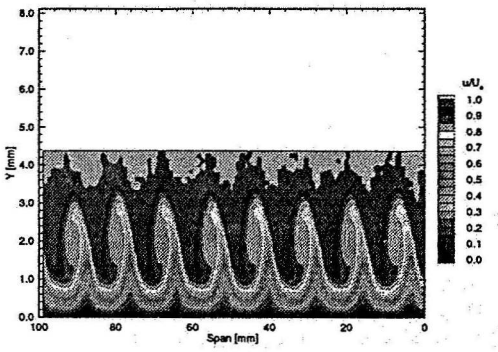


Figure 3: Streamwise velocity contours at $x/c = 0.45$, $Re_c = 2.4 \times 10^6$. A full-span array of 6 $\mu$m roughness with 12 mm spacing is at $x/c = 0.023$.

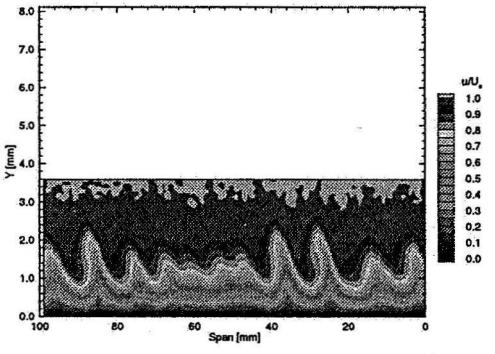


Figure 2: Streamwise velocity contours at $x/c = 0.45$, $Re_c = 3.0 \times 10^6$. No artificial roughness.

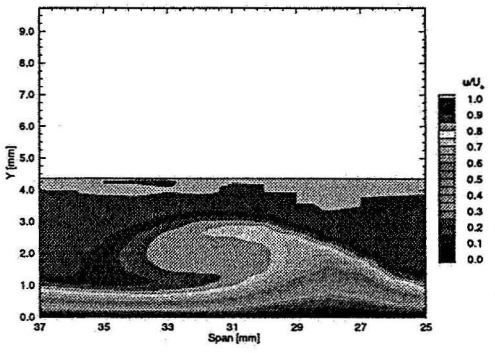


Figure 4: Single stationary crossflow vortex isolated from Figure 3 and plotted on a 1:1 scale.

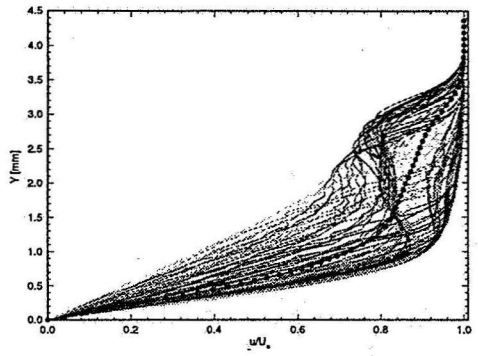


Figure 5: Spanwise array of boundary-layer profiles at $x/c = 0.45$, $Re_c = 2.4 \times 10^6$. A full-span array of 6 $\mu$m roughness with 12 mm spacing is at $x/c = 0.023$. The dots indicate the mean of the profiles.

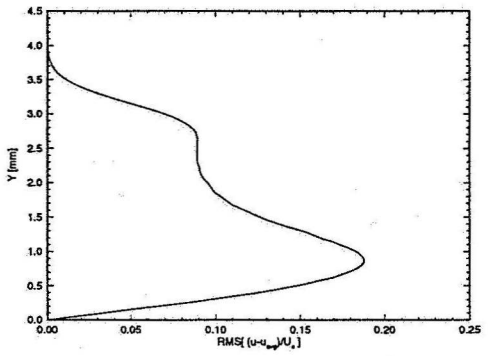


Figure 7: Stationary crossflow mode shape at $x/c = 0.45$, $Re_c = 2.4 \times 10^6$. A full-span array of 6 $\mu$m roughness with 12 mm spacing is at $x/c = 0.023$.

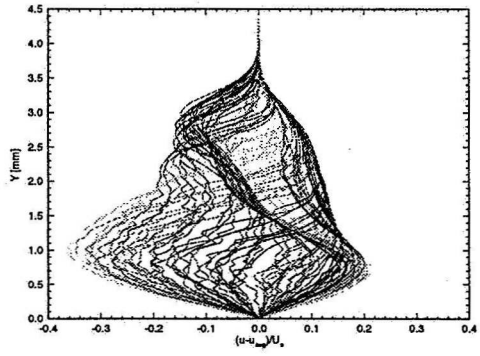


Figure 6: Spanwise array of disturbance profiles at $x/c = 0.45$, $Re_c = 2.4 \times 10^6$. A full-span array of 6 $\mu$m roughness with 12 mm spacing is at $x/c = 0.023$.

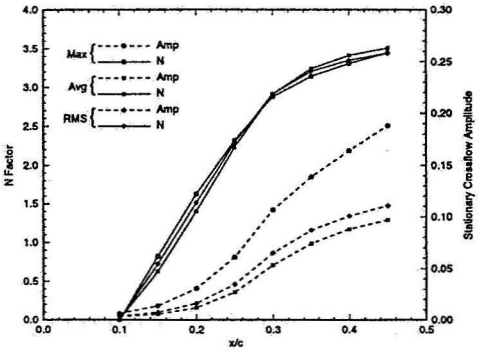


Figure 8: Disturbance amplitude distribution at $Re_c = 2.4 \times 10^6$. A full-span array of 6 $\mu$m roughness with 12 mm spacing is at $x/c = 0.023$. The reference point for the $N$-factor calculations is $x/c = 0.10$.

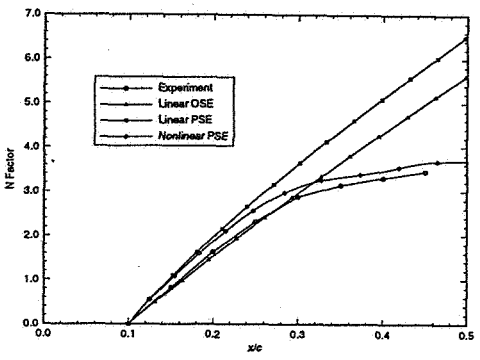


Figure 9: Measured and theoretical $N$-factor for $Re_c = 2.4 \times 10^6$. A full-span array of 6 $\mu$m roughness with 12 mm spacing is at $x/c = 0.023$. The reference point for the $N$-factor calculations is $x/c = 0.10$.

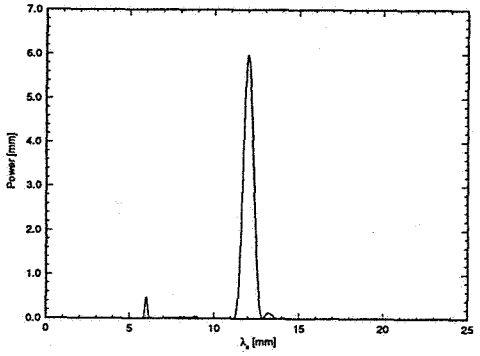


Figure 11: FFT power spectrum of spanwise hot-wire scan at $x/c = 0.45$, $Re_c = 2.4 \times 10^6$, $y = 0.9$ mm. A full-span array of 6 $\mu$m roughness with 12 mm spacing is at $x/c = 0.023$.

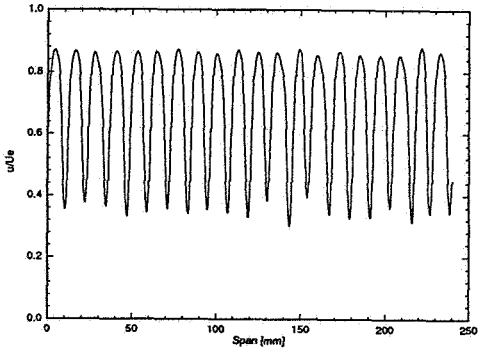


Figure 10: Spanwise hot-wire scan at $x/c = 0.45$, $Re_c = 2.4 \times 10^6$, $y = 0.9$ mm. A full-span array of 6 $\mu$m roughness with 12 mm spacing is at $x/c = 0.023$.

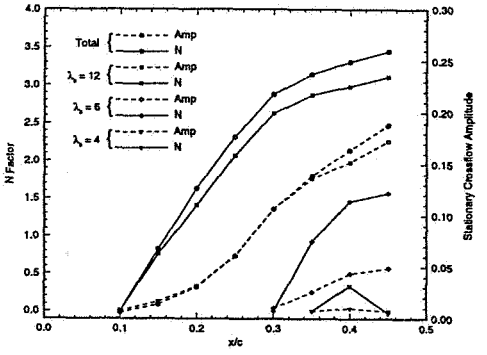


Figure 12: Total and single-mode amplitude distribution at $Re_c = 2.4 \times 10^6$. A full-span array of 6 $\mu$m roughness with 12 mm spacing is at $x/c = 0.023$. $N$-factors are relative to the point at which the disturbance is first detected.